

Second-harmonic generation in metallic nanoparticles: Clarification of the role of the surfaceCristian Ciraci,^{1,*} Ekaterina Poutrina,¹ Michael Scalora,² and David R. Smith¹¹*Center for Metamaterials and Integrated Plasmonics, and Department of Electrical and Computer Engineering, Duke University, Durham North Carolina 27708, USA*²*C. M. Bowden Research Facility, U.S. Army, RDECOM, Redstone Arsenal, Alabama 35803, USA*

(Received 19 June 2012; revised manuscript received 14 August 2012; published 27 September 2012)

We present a numerical investigation of the second-order nonlinear optical properties of metal-based metamaterial nanoresonators. The nonlinear optical response of the metal is described by a hydrodynamic model, with the effects of electron pressure in the electron gas also taken into account. We show that as the pressure term tends to zero the amount of converted second-harmonic field tends to an asymptotic value. In this limit it becomes possible to rewrite the nonlinear surface contributions as functions of the value of the polarization vector inside the bulk region. Nonlocality thus can be incorporated into numerical simulations without actually utilizing the nonlocal equation of motion or solving for the rapidly varying fields that occur near the metal surface. We use our model to investigate the second-harmonic generation process with three-dimensional gold nanoparticle arrays and show that nanocrescents can easily attain conversion efficiencies of $\sim 6.0 \times 10^{-8}$ for pumping peak intensities of a few tens of MW/cm².

DOI: [10.1103/PhysRevB.86.115451](https://doi.org/10.1103/PhysRevB.86.115451)

PACS number(s): 42.65.Ky, 81.05.Xj, 78.67.Pt, 73.20.Mf

I. INTRODUCTION

Metamaterials are artificially structured media whose collective electromagnetic properties can differ markedly from those displayed by the individual components. The advent of metamaterials has introduced a paradigm shift in the concept of what constitutes a material and what determines its fundamental electromagnetic and other physical properties. The possibility of tailoring magnetic and electric material responses at will, rather than merely exploiting materials provided by nature, has enabled the pursuit of unusual electromagnetic properties, such as invisibility¹ and negative refractive index.²

Without a doubt, metamaterials constitute novel and interesting linear media that have provided a venue to explore otherwise inaccessible concepts. Yet, artificial materials in the context of nonlinear optical media may offer even greater opportunities, since the inherent local field inhomogeneities associated with metamaterial inclusions can translate into large enhancement of the local field and significant lowering of the nonlinear thresholds.

Nonlinear metamaterial composites have been analyzed both theoretically and experimentally in the microwave and near-infrared regions of the spectrum.^{3–5} For such materials, one may apply an analytical homogenization model that leads to closed-form expressions for the effective nonlinear susceptibilities,⁶ placing the design of nonlinear metamaterials on an equal footing with linear metamaterials. In addition, numerical retrieval approaches have been developed that allow precise values to be ascribed to the effective nonlinear susceptibilities for a composite metamaterial comprising both structured inclusions as well as embedded nonlinear elements.^{7,8}

The most common metamaterial designs have made use of conducting metal inclusions that function as subwavelength electrical circuits. At low frequencies, metals behave as conductors, and, thus, metal inclusions can be conceptually divided into inductive, capacitive, and resistive regions, with a resonance frequency determined by the inductance and capac-

itance in the usual manner. If any of these circuit parameters are made nonlinear—through the introduction of an actual lumped component such as a varactor diode or an inherently nonlinear crystal embedded into the capacitive region of the inclusion—the effective circuit then produces a nonlinear response to the driving electric or magnetic field (depending on how the wave couples to the inclusion). Applying analytical or retrieval techniques on such a structure yields adequate effective medium values for the linear constitutive tensor elements, as well as for the tensor elements of the nonlinear susceptibility terms. A nonlinear metamaterial is advantageous in that nonlinear thresholds may be significantly lowered, often irrespective of the linear properties of the composite. That is, the linear and nonlinear responses of a nonlinear metamaterial can be designed with considerable independence, allowing customized anisotropy and other properties that may be used to improve the efficiency of nonlinear applications.

Nonlinear metamaterials based on metals are, thus, appealing for potential use in nonlinear optical applications at infrared, visible, and ultraviolet wavelengths. However, a simple scaling of the geometrical parameters of metamaterial inclusions from microwave to visible frequencies, for example, is usually not sufficient to create a viable nonlinear optical metamaterial. At frequencies above a few terahertz, metal response changes from conductor-like to dielectric-like, with considerable absorption occurring as the electromagnetic radiation extends further and further into the metal. Though the electrical circuit properties of metal inclusions persist at visible wavelengths, the inertia of the charge carriers becomes an increasingly dominant contribution to the inductance, and absorption increases significantly.⁹ The design of metal optical metamaterials—where optical is roughly defined as being above 10–12 THz—requires a different approach, with different applications being favored.

In addition to field enhancement being a useful mechanism in optical metamaterials, the intrinsic nonlinearity of metals makes metal-based nonlinear optical metamaterials an interesting possibility. For example, values of $\chi^{(3)}$ for metals at optical wavelengths are competitive with most materials.

$\chi^{(3)}$ of gold is $5.4 \times 10^{-19} \text{ m}^2/\text{V}^2$, somewhat lower than semiconductors such as silicon ($\chi^{(3)} = 2.0 \times 10^{-18} \text{ m}^2/\text{V}^2$) but larger than other common crystals such as diamond ($\chi^{(3)} = 1.8 \times 10^{-21} \text{ m}^2/\text{V}^2$) or Al_2O_3 ($\chi^{(3)} = 2.2 \times 10^{-22} \text{ m}^2/\text{V}^2$).¹⁰ Moreover, though metals are centrosymmetric and do not possess an inherent $\chi^{(2)}$ nonlinearity, the surface of a metal can break the symmetry and provide a mechanism for an effective $\chi^{(2)}$ nonlinearity. The homogenized $\chi^{(2)}$ nonlinear response of a metal, thus, becomes highly dependent on its geometry, making it inherently a metamaterial construct. In all cases, the large absorption associated with metals suggests nanostructuring as a means of optimizing the nonlinear effects while minimizing propagation within the metal. As we show here, nonlinear metal-based metamaterials can accomplish these goals.

The origin of the nonlinearity in metals arises from the response of both bound and free electrons. In particular, for the visible/near-IR part of the spectrum, the nonlinear response of thick metal layers may be attributed mostly to free electrons, with Lorentz (magnetic) and quadrupolar contributions from bound charges becoming increasingly important at shorter wavelengths. The interest in nonlinear interactions at metal surfaces dates back to the beginning of nonlinear optics.^{11–17} Optical second-harmonic generation from a silver slab was first observed in 1965.^{18,19} Since then, numerous experimental studies have been published,^{20–24} with a variety of phenomenological^{25–33} and microscopic approaches^{34–37} developed to analyze the second-harmonic response of metal structures.

Recent research in plasmonic phenomena has stimulated renewed interest in the nonlinear optical properties of metals. In particular, a steady stream of works concerning harmonic generation from metallic nanostructures, such as hole arrays in a metallic substrate,^{38–43} metalodielectric multilayer structures,^{44,45} Au nanoantennas,^{46,47} and periodic nanostructured metal films,^{48,49} have been published recently. Second-harmonic generation has also been observed experimentally from ordered arrays of split-ring resonators,^{50,51} as well as from a variety of single nanoparticles^{52–56} and nanoparticle arrays with varying geometries.^{57–69} On the theoretical side, Zeng *et al.* readapted the free-electron theory of second-harmonic generation to arbitrary shaped metal nanoparticles.⁷⁰ Scalora *et al.* have considered a dynamic description based on the hydrodynamic model and taken into account bound electron contributions to the second- and third-harmonic generation in the ultrashort pulse regime.⁷¹

It should be emphasized that metals contain both volume and surface nonlinear contributions,²⁸ and it is generally not possible to entirely separate the two. The separation becomes even more ambiguous for subwavelength nanolayers or nanoparticles, where the field can penetrate the metal itself so the nonlinear response may be distributed inside the volume. Under these circumstances the shape of the nanoparticle acquires a more crucial role in determining the nonlinear response of the metal. Moreover, nonlinear surface contributions are strictly related to the response of the electrons within the Thomas-Fermi screening length ($\lambda_{\text{TF}} \sim 1 \text{ \AA}$ for gold) from the surface, which introduces a crucial microscopic scale to the problem. Thus, solving for the optical fields in the macroscopic realm, which vary on

the order of several hundred nanometers, can rapidly result in considerable numerical complexity.

In this work we perform an analysis of second-harmonic generation in plasmonic systems of arbitrary shape. We, first, summarize the hydrodynamic model that describes the nonlinear optical response of the metal, including the effects of quantum pressure associated with the electron gas. A numerical analysis of the resulting nonlocal and nonlinear problem is performed, with particular emphasis on surface effects. In particular, we numerically investigate the nonlinear response at the metal surface as the electron pressure tends to zero, thus establishing an unambiguous bridge to the *free-electron limit*, in which the pressure is completely neglected. In a recent work⁷² we provided a formula expressing the nonlinear surface contribution in terms of the polarization vector in the bulk regions. Here we show a detailed comparison with the full resolution of nonlocal and nonlinear equations. We then numerically investigate second-harmonic generation arising from a variety of three-dimensional nanoparticle arrays and show the impact of specific geometries, such as nanocrescents, on the enhancement of conversion efficiencies.

II. MODEL

A description for the polarization inside the metal is given by the hydrodynamic model. Here we recall the most salient elements of the theory and refer the reader to Refs. 73, 35, and 71 for further details.

The electron fluid density, $n(\mathbf{r}, t)$, and the current density, $\mathbf{J} = en\mathbf{v}$, satisfy Euler's equation,

$$m_e^* n \left[\frac{\partial \mathbf{v}}{\partial t} + (\mathbf{v} \cdot \nabla) \mathbf{v} + \gamma \mathbf{v} \right] = en\mathbf{E} + en\mathbf{v} \times \mathbf{B} - \nabla p, \quad (1)$$

along with the continuity equation,

$$\nabla \cdot \mathbf{J} = -e\dot{n}, \quad (2)$$

where the dot represents the partial derivative with respect to time, m_e^* is the effective electron mass, γ is the electron collision rate, \mathbf{v} is the electron velocity field, and p is the electron pressure which, for a three-dimensional gas, is given by^{71,74}

$$p(\mathbf{r}, t) = p_0 \left[\frac{n(\mathbf{r}, t)}{n_0} \right]^{5/3}, \quad (3)$$

where $p_0 \simeq n_0 E_F$ (E_F is the Fermi energy and n_0 is the equilibrium charge density). Combining Eqs. (2), (1), and (3), and taking into account $\dot{\mathbf{P}} = \mathbf{J}$, one finds that the free-electron polarization \mathbf{P} satisfies the following equation⁷¹:

$$\begin{aligned} \ddot{\mathbf{P}} + \gamma \dot{\mathbf{P}} = & \frac{n_0 e^2}{m_e^*} \mathbf{E} - \frac{e}{m_e^*} \mathbf{E} (\nabla \cdot \mathbf{P}) + \frac{e}{m_e^*} \dot{\mathbf{P}} \times \mathbf{B} \\ & - \frac{1}{n_0 e} [(\nabla \cdot \dot{\mathbf{P}}) \dot{\mathbf{P}} + (\dot{\mathbf{P}} \cdot \nabla) \dot{\mathbf{P}}] + \frac{5 E_F}{3 m_e^*} \nabla (\nabla \cdot \mathbf{P}) \\ & - \frac{10}{9} \frac{E_F}{e n_0 m_e^*} (\nabla \cdot \mathbf{P}) \nabla (\nabla \cdot \mathbf{P}). \end{aligned} \quad (4)$$

In calculating Eq. (4), only first- and second-order terms have been retained. Equation (4) summarizes the electron fluid response under the influence of the electromagnetic field. In addition to the linear Drude response, we have the nonlinear

Coulomb term (referred to as quadrupole-like term by virtue of its form), proportional to $\mathbf{E}(\nabla \cdot \mathbf{P})$, the magnetic Lorentz force contribution, $\mathbf{P} \times \mathbf{B}$, the convective terms $(\nabla \cdot \mathbf{P})\mathbf{P}$ and $(\mathbf{P} \cdot \nabla)\mathbf{P}$, the linear nonlocal pressure term proportional to $\nabla(\nabla \cdot \mathbf{P})$, and the nonlinear pressure term $(\nabla \cdot \mathbf{P})\nabla(\nabla \cdot \mathbf{P})$.

In order to calculate the expressions for the fundamental and second-harmonic polarization, we expand all fields in a perturbative manner,

$$\begin{aligned}\mathbf{E}(\mathbf{r}, t) &= \mathbf{E}_1(\mathbf{r})e^{-i\omega t} + \mathbf{E}_2(\mathbf{r})e^{-2i\omega t} + \dots, \\ \mathbf{H}(\mathbf{r}, t) &= \mathbf{H}_1(\mathbf{r})e^{-i\omega t} + \mathbf{H}_2(\mathbf{r})e^{-2i\omega t} + \dots, \\ \mathbf{P}(\mathbf{r}, t) &= \mathbf{P}_1(\mathbf{r})e^{-i\omega t} + \mathbf{P}_2(\mathbf{r})e^{-2i\omega t} + \dots,\end{aligned}\quad (5)$$

where the time dependence has been explicitly indicated. Considering terms up to the second order, we obtain the following set of equations:

$$\beta^2 \nabla(\nabla \cdot \mathbf{P}_1) + (\omega^2 + i\omega\gamma)\mathbf{P}_1 = -\frac{n_0 e^2}{m_e^*} \mathbf{E}_1, \quad (6a)$$

$$\beta^2 \nabla(\nabla \cdot \mathbf{P}_2) + (4\omega^2 + 2i\omega\gamma)\mathbf{P}_2 = -\frac{n_0 e^2}{m_e^*} \mathbf{E}_2 + \mathbf{S}_{\text{NL}}, \quad (6b)$$

where $\beta^2 = (5/3)E_F/m_e^*$ and the nonlinear source, \mathbf{S}_{NL} , is given by

$$\begin{aligned}\mathbf{S}_{\text{NL}} &= \frac{e}{m_e^*} \mathbf{E}_1 (\nabla \cdot \mathbf{P}_1) + \frac{i\omega e}{m_e^*} \mathbf{P}_1 \times \mathbf{B}_1 \\ &\quad - \frac{\omega^2}{n_0 e} [(\nabla \cdot \mathbf{P}_1)\mathbf{P}_1 + (\mathbf{P}_1 \cdot \nabla)\mathbf{P}_1] \\ &\quad + \frac{10}{9} \frac{E_F}{en_0 m_e^*} (\nabla \cdot \mathbf{P}_1) \nabla(\nabla \cdot \mathbf{P}_1).\end{aligned}\quad (7)$$

The quantity β is proportional to the Fermi velocity v_F and, consequently, to the Thomas-Fermi screening length $\lambda_{\text{TF}} = v_F/\omega_p$, with ω_p being the plasma frequency. Equations (6) with Eq. (7) describe the fundamental and second-harmonic polarization vectors, respectively, and hold under the assumption that the fundamental fields are not affected by the generated harmonic (nondepleted pump approximation). However, should one desire to calculate the self-consistent field interaction, the necessary terms may be taken into account by modifying Eq. (6a).

Equations (6) are solved along with Maxwell's equations that, in the framework of harmonic propagation, read⁷⁵

$$\nabla \times \nabla \times \mathbf{E}_1 - k_1^2 \mathbf{E}_1 = \mu_0 \omega^2 \mathbf{P}_1, \quad (8a)$$

$$\nabla \times \nabla \times \mathbf{E}_2 - k_2^2 \mathbf{E}_2 = \mu_0 4\omega^2 \mathbf{P}_2, \quad (8b)$$

where $k_1 = \omega/c$ and $k_2 = 2\omega/c$, with c the light velocity in vacuum.

The polarization defined by Eqs. (6) contain linear, nonlocal contributions arising from the electron pressure of the form $\beta^2 \nabla(\nabla \cdot \mathbf{P})$. This term has been shown to introduce significant modifications in the optical properties of subnanometer-gap metal-based systems.⁷⁶ It has also been predicted to be responsible for an unusual, resonant-like phenomenon for nanowires only a few nanometers in diameter.⁷⁷⁻⁷⁹ More generally, this term takes into account variations of the electric field occurring in a region of the order of λ_{TF} in the vicinity of the metal surface, where electron-electron interactions become significant. The presence of spatial derivatives (nonlocality)

in the description of the polarization vector requires the specification of additional boundary conditions to solve the electromagnetic boundary value problem.^{80,81}

The choice of additional boundary conditions required at an interface is a delicate problem that remains an unsettled topic in the literature. From the physical point of view, the presence of a pressure in the electron fluid enables the existence of *longitudinal waves*, in which the electric field is aligned with the propagation vector, along with the conventional *transverse waves*. That is, an incident field can excite two independent waves inside the metal. The well-known Maxwell's boundary conditions are not sufficient to uniquely define the amplitudes of these possible waves. In terms of a hydrodynamic description, the number of additional boundary conditions depends on the given equilibrium charge density profile at the metal boundaries. For our problem, we assume the equilibrium electron density to have a step-function profile that vanishes outside the metal. In this case, only one additional boundary condition is required to supplement Eqs. (6) to obtain a unique solution.⁸² Intuitively, a simple boundary condition may be ascertained by considering the meaning of our equations. From a macroscopic point of view, Maxwell's equations require the normal component of the vector $\mathbf{D} = \epsilon_0 \mathbf{E} + \mathbf{P}$ to be continuous across the interface, if no external charges are present, while the normal component of the electric field $\hat{\mathbf{n}} \cdot \mathbf{E}$ is discontinuous because of the induced surface charges ($\hat{\mathbf{n}}$ is a unit vector normal to the boundary). However, the nonlocal, linear terms in Eqs. (6b) account for a microscopic description of the charge behavior at the surfaces of the metal region. It is then legitimate to impose the continuity of the normal component of the electric field across the interface, which means it must be $\hat{\mathbf{n}} \cdot \mathbf{P} = \mathbf{0}$ at the metal-air interface. On the other hand, the tangential component of the polarization vector, $\hat{\mathbf{n}} \times \mathbf{P}$, is, in general, nonzero. More formally, the same result may be derived from the continuity equation and Gauss's theorem. In this case, one obtains that $\hat{\mathbf{n}} \cdot \mathbf{J} = \mathbf{0}$ at the boundary.^{78,82}

Within this context the macroscopic discontinuity of $\hat{\mathbf{n}} \cdot \mathbf{E}$ translates into a rapid variation of the microscopic fields within the neighborhood of the boundary and the term $\nabla \cdot \mathbf{P}$ will give indeed the distribution of the induced charge along the metal-air transition. Equations (6) coupled to Eqs. (8) are numerically solved using the finite-element method implemented in the commercial software COMSOL Multiphysics.⁸⁴ The weak form of the nonlocal contribution derived in the appendix has been used.

A. Second-harmonic generation from a metal nanowire

To illustrate the nature of the various nonlinear processes that derive from the hydrodynamic response model, we consider a p -polarized plane wave incident on a metal wire of circular cross section as depicted in Fig. 1(a). It is interesting to assess the influence of the linear pressure term on the induced charge density. One would expect the electron distribution to be zero in the bulk region and rapidly varying near the metal surface, where it should reach its maximum value. The induced charge density $n = \frac{1}{e} \nabla \cdot \mathbf{P}$ is shown in Fig. 2, for different values of β , along the direction normal to the metal-air interface. We note that the region where the variation occurs is of order of $\lambda_{\text{TF}} \sim 0.1$ nm.

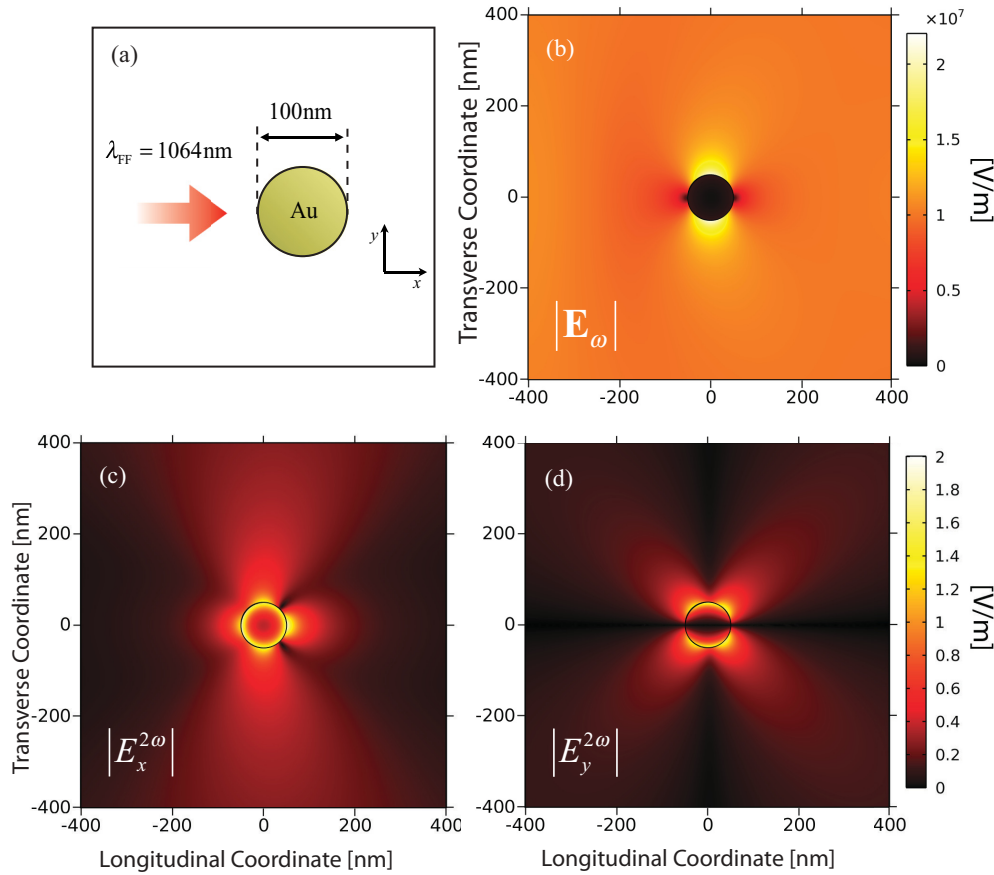


FIG. 1. (Color online) (a) A plane wave of wavelength $\lambda = 1064$ nm impinges on a gold wire of diameter $d = 100$ nm. (b) Absolute value of the fundamental electric field. The second-harmonic field components obtained by solving Eqs. (8) and (6) are shown in (c) and (d). The following values were used: $m_e^* = m_e$, $n_0 = 5.7 \times 10^{22}$ cm $^{-3}$, $\gamma = 1.07 \times 10^{14}$ s $^{-1}$, and $E_F = 5.5$ eV.

As the fundamental wave interacts with the metal wire, a second-harmonic field given by the nonlinear polarization of Eq. (6b) and Eq. (7) is generated (see Fig. 1). It is useful to closely examine the contribution of the various nonlinear source terms to the generated second harmonic. In Fig. 3 we show the generated second-harmonic field patterns corresponding to each of the nonlinear terms in Eq. (6b), with all other nonlinear sources turned off. The corresponding second-harmonic scattered powers, Q_{SH} , are also indicated in

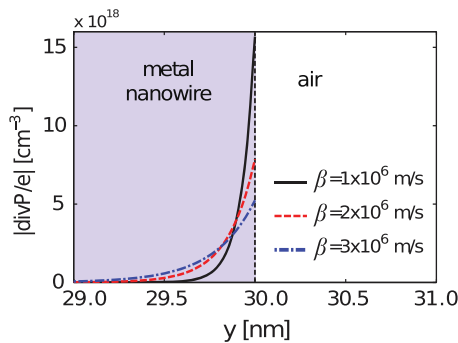


FIG. 2. (Color online) Electron density profile at the metal-air interface for different values of β for the fundamental field. The geometry was discretized by a triangular mesh with a 0.025-nm maximum element size at the metal surface.

Fig. 3. If all the nonlinear sources are present simultaneously the total converted power is $Q_{SH} = 1.53 \times 10^{-10}$ W, a value almost twice the sum given by each of the individual contributions. This means that the terms interfere, and each term may establish a nonlinear interaction channel that could be amplified or reduced by the other terms. Consequently, it is not easy to estimate the impact of an individual term on the generated field, which, in general, will depend on the geometrical configuration and other parameter choices.

It is also useful to determine the relative second harmonic contributions from the surface and the bulk of the geometry. With respect to Eq. (7), surface terms may be identified as being proportional to $\nabla \cdot \mathbf{P}_1$, a term that is nonzero only near the surface. That is, the Coulomb (quadrupole-like) and pressure terms, and the first of the convective terms, may be taken to be purely surface terms, while the Lorentz force is a purely bulk term. On other hand, the convective term proportional to $(\mathbf{P}_1 \cdot \nabla)\mathbf{P}_1$ contains both surface and bulk contributions. In Fig. 4 we plot the absolute values of the transverse and normal component of the vectors $(\nabla \cdot \mathbf{P}_1)\mathbf{P}_1$ and $(\mathbf{P}_1 \cdot \nabla)\mathbf{P}_1$, respectively. Near the surface the normal components of both terms behave similarly, while only the latter does not vanish in the bulk region. An important difference can be observed in the transverse component, where there is no surface contribution for the term $(\mathbf{P}_1 \cdot \nabla)\mathbf{P}_1$. These distinctions qualitatively hold for different types of nanoparticles. However, the precise

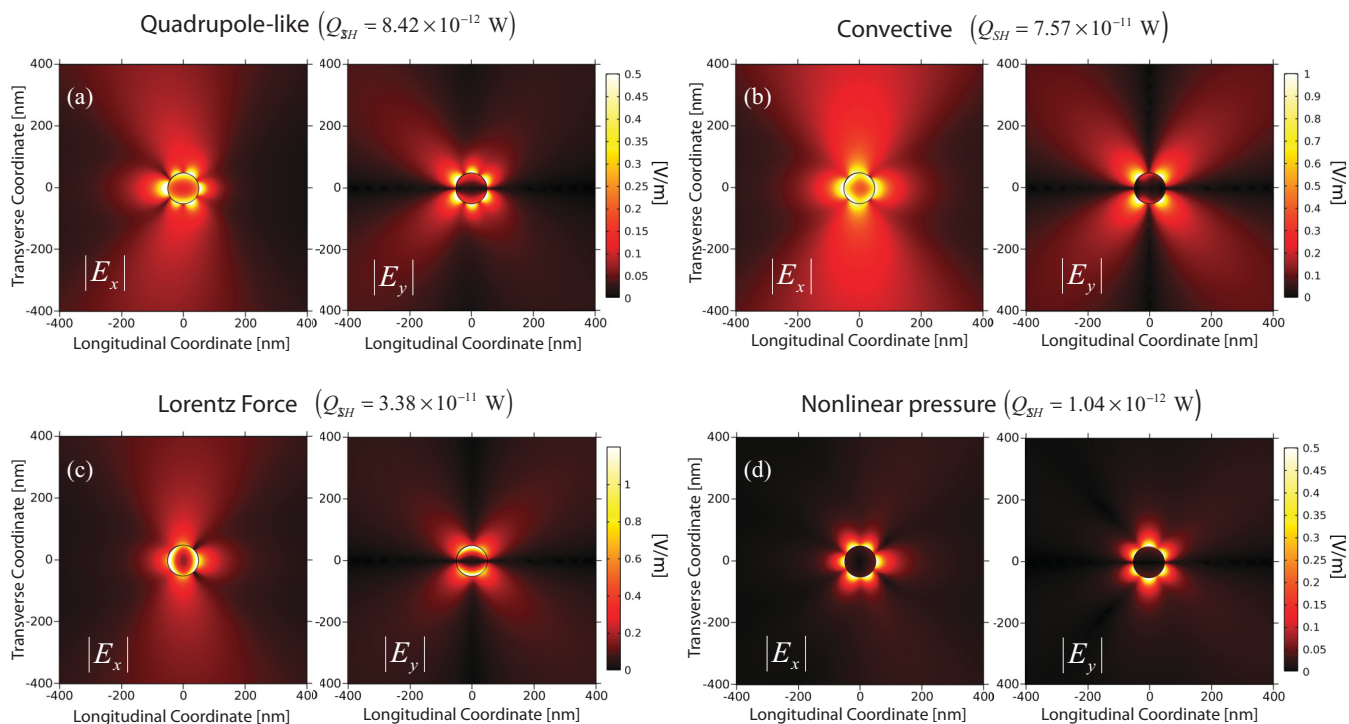


FIG. 3. (Color online) Second-harmonic field patterns generated by the different nonlinear sources of Eq. (6b) for the geometry in Fig. 1. The total scattered second-harmonic power Q_{SH} is shown for a pump peak intensity of ~ 15 MW/cm². The field patterns were calculated by considering only the second-harmonic source term of interest and turning off all others.

fraction associated with surface or bulk contributions depends on the specific geometry under consideration.

B. Free-electron limit

The hydrodynamic description of the electrons inside a metal gives a fairly accurate description of linear and nonlinear processes occurring at the surface of metallic structures. Though microscopic interactions are described by a very simplistic model, the simultaneous manifestation of multiple scales (the angstrom length scale of the electron-electron interactions, on the one hand, and the micron scale of particle-field interaction, on the other hand) makes the numerical resolution of the electromagnetic problem quite complex and ordinarily necessitates considerable computational resources even for particles whose dimensions are a few tens of nanometers. In Ref. 72 we showed that it is possible to express the nonlinear surface contribution in terms of the bulk polarization, without having to solve the nonlocal equations. As already pointed out by Sipe *et al.*,³⁵ if the electron pressure is simply dropped off by the equations, the hydrodynamic theory of second-harmonic generation becomes inherently ambiguous. This is because products of the form $(\nabla \cdot \mathbf{P})\mathbf{E}$ are not well defined if both \mathbf{P} and \mathbf{E} are discontinuous.⁷²

In early works this problem was circumvented by introducing phenomenological coefficients to determine the weight of the different nonlinear contributions,³⁴ or through an effective plasma frequency,³⁵ that incorporate the details of the charge distribution near the surface, an effect that was neglected in Ref. 70. We have numerically analyzed the effect of the linear pressure on the amount of converted second-harmonic energy.

This is shown in Fig. 5 where the total second-harmonic scattered power is plotted as a function of the inverse of β . Figure 5 shows that the total second-harmonic generation converges to an asymptotic value as β tends toward zero. Typical reported values for β are on the order of 10^6 m/s and correspond to the flat region of the curve, where the actual converted energy does not differ too much from its asymptotic value. Exploring the limit for $\beta \rightarrow 0$ seems, then, a very good way to get an approximate solution that includes the effects of nonlocality, but without having to solve the complex nonlocal equations. Note that this procedure differs totally from assuming β is identically zero.

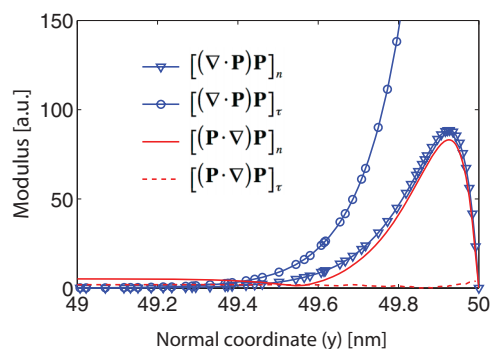


FIG. 4. (Color online) Comparison between the convective source terms calculated for the nanowire of Fig. 1. The nanowire is centered at the origin and the fields are taken along the direction $x = 0$ in the neighborhood of the metal-air interface ($y = 50$ nm). Note that the direction of interest is normal to the metal boundary.

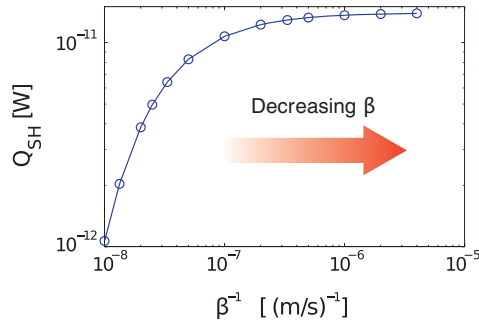


FIG. 5. (Color online) Total second-harmonic scattered power as a function of the inverse of the parameter β for a gold nanowire of diameter $d = 30$ nm.

In this limit the surface contributions to the second-harmonic polarization may be approximated by an effective nonlinear current sheet at the surface of the nanoparticle given by⁷²

$$\mathbf{K}_{\text{NL}} = \frac{i\omega}{n_0 e} \left[\hat{\mathbf{t}}(P_1^\perp P_1^\parallel) + \hat{\mathbf{n}} \frac{1}{2} \frac{3\omega + i\gamma}{2\omega + i\gamma} (P_1^\perp)^2 \right], \quad (9)$$

where the unit vectors $\hat{\mathbf{n}}$ and $\hat{\mathbf{t}}$ are normal and parallel to the metal interface, respectively, and $P_1^\perp = \hat{\mathbf{n}} \cdot \mathbf{P}_1$ and $P_1^\parallel = \hat{\mathbf{t}} \cdot \mathbf{P}_1$. These currents are related to the polarization values in the bulk region and do not require the resolution of nonlocal equations. This approach provides a good description of the second-harmonic generation process that may be easily implemented for full three-dimensional (3D) simulations. However, since in this local description of surface nonlinear contributions, the derivatives in the direction parallel to the surface are neglected, Eq. (9) is not expected to hold if, for example, one considers geometries with sharp asperities, in which field derivatives can be very important.⁷² More generally, the approximation is valid as long as nonlocal effects do not change the linear response of the system.

As a test case, we consider second-harmonic generation from a thick metal film. In Ref. 84 experimental data for a pump field tuned at 1064 nm and incident on a 400-nm silver film are reported for three different incident/detected polarization configurations: (i) TM-incident and TM-detected polarization; (ii) TE-incident and TM-detected polarization, and (iii) 45°-incident and TE-detected polarization. In Fig. 6 we compared the results obtained using Eq. (9) with those obtained through the full resolution of Eqs. (6). For completeness the experimental data are also reported. Both simulation results agree qualitatively and quantitatively very well in all cases. A slight difference between the two numerical results may be observed for the case of TM-incident and TM-detected polarization [see Fig. 6(a)]. This slight difference arises because in that configuration the impact of the electron pressure is more significant. However, the qualitative agreement is still very good.

III. THREE-DIMENSIONAL NANOPARTICLES

In the previous paragraph we showed how second-harmonic generation may be handled without solving the entire electromagnetic-hydrodynamic problem. That is, the

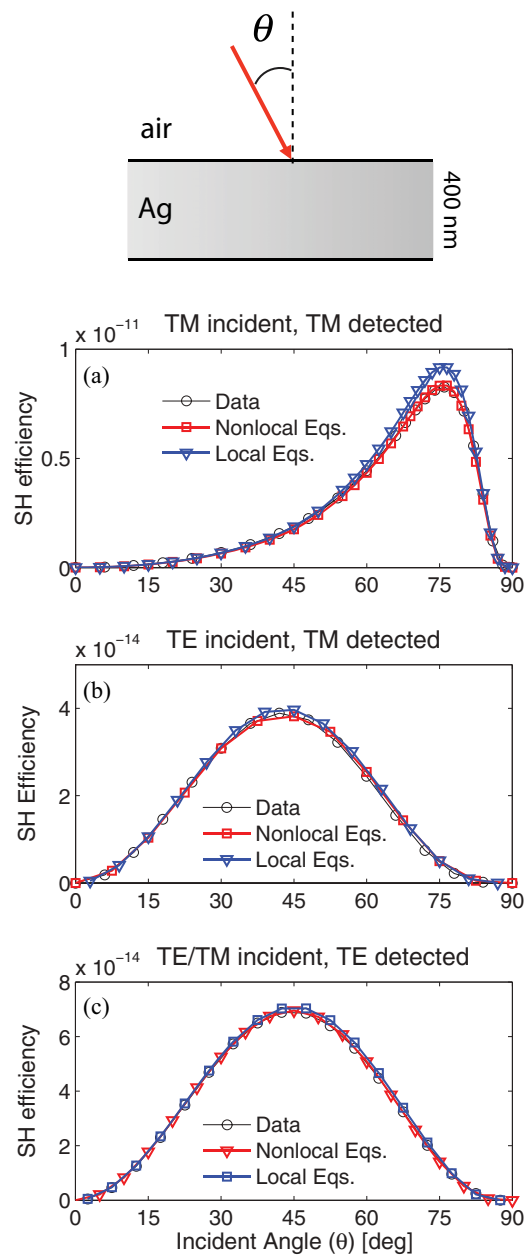


FIG. 6. (Color online) Second-harmonic conversion efficiency for a silver film as a function of the incident angle θ as depicted in the inset, under various pumping/detection polarization conditions. The fundamental field is tuned at the wavelength $\lambda = 1064$ nm. Experimental data are taken from Ref. 84, where the average peak intensity is estimated about 80 MW/cm². The shapes of both theoretical curves agree well with the experimental data in all cases, if we choose the following incident peak intensities: (a) ~ 85 MW/cm², (b) ~ 60 MW/cm², and (c) ~ 110 MW/cm². The effective electron mass has been fixed to $m_e^* = 0.65m_e$ and $n_0 = 3.5 \times 10^{22}$ cm⁻³, $\gamma = 4.6 \times 10^{13}$ s⁻¹, and $E_F = 5.5$ eV.

volume sources are calculated by assuming β identically zero, while the surface nonlinear currents are given by Eq. (9). In this section we will use this approach to study 3D gold nanoparticles. For the sake of simplicity, we assume the nanoparticles are surrounded by air. The structure studied extends periodically in the x and y directions, as depicted

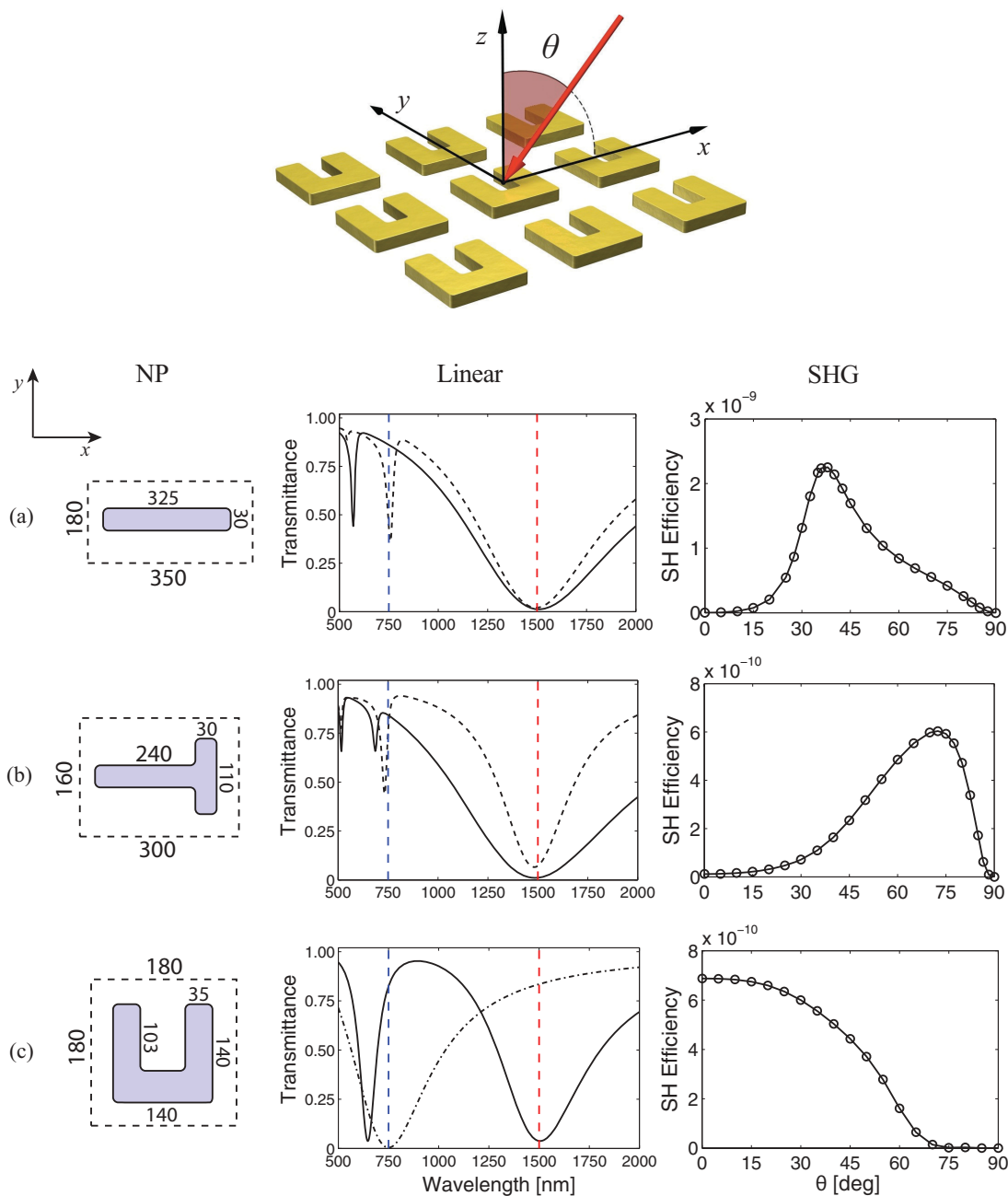


FIG. 7. (Color online) Second-harmonic conversion efficiency for different 3D gold nanoparticles. All the particles are 20 nm thick and the geometrical parameters have been chosen to have a resonance around $\lambda_{FF} = 1.5 \mu\text{m}$, where the fundamental field is tuned. The linear transmissions at normal incidence (solid line) for the variety of nanoparticles are shown in the second column. In (a) and (b) the transmission at oblique incidence (dashed line) has been calculated for $\theta = 40$ and $\theta = 70$, respectively. The transmission for an incident electric field polarized along the y direction is also shown for the U-shaped nanoparticle (dot-dash line). The vertical dotted lines indicate the fundamental and the second-harmonic wavelength, respectively. The second-harmonic conversion efficiency as a function of the incident angle θ has been calculated using Eq. (9) to take into account the nonlinear surface contribution. The pumping electric field is p polarized ($E_y = 0$) with a peak intensity of $\sim 55 \text{ MW/cm}^2$. The following values for the parameters have been used: $m_e^* = m_e$, $n_0 = 5.7 \times 10^{22} \text{ cm}^{-3}$, and $\gamma = 1.07 \times 10^{14} \text{ s}^{-1}$.

in the inset of Fig. 7, so only a single unit cell is needed in the computational space. To avoid possible numerical artifacts due to the field localization near metal corners, we considered rounded corner geometries with a radius of curvature of 5 nm. The geometrical parameters were chosen so the nanoparticles would display a resonance around $\lambda_{FF} = 1.5 \mu\text{m}$, where the fundamental field is tuned.

Our results are summarized in Fig. 7 for the different kinds of nanoparticles. The conversion efficiencies assume an average pump intensity of $\sim 55 \text{ MW/cm}^2$ with the electric pumping field lying on the xz plane. We find qualitatively good agreement with the experimental data of Ref. 58, where second- and third-harmonic generation were experimentally investigated for a variety of gold nanoparticles. The authors considered

arrays of unit cells ranging from 300 to 600 nm constituted of gold nanoparticles deposited on a thick glass substrate under normal pump incidence. Even if a quantitative comparison between our simulations and the experimental data cannot be made, the relative efficiencies normalized with respect to the U-shaped nanoparticle efficiency are, nevertheless, in very good agreement. For the U-shaped nanoparticle at normal incidence, we find a conversion efficiency of $\sim 6.9 \times 10^{-10}$. This should be compared to $\sim 2.0 \times 10^{-11}$ of the experimental data.^{58,85} The T-shaped nanoparticle shows an efficiency of $\sim 1.1 \times 10^{-11}$ for $\theta = 0^\circ$, or about the 1.7% with respect of the U-shaped nanoparticle (2.1% for the experimental data), and the I-shaped nanoparticle has a ~ 0 conversion efficiency, as one might expect due to the absence of symmetry breaking. It is interesting to observe the second-harmonic conversion efficiency as a function of pumping angle θ for the three kinds of nanoparticles. The geometry is depicted in the third column of Fig. 7. While the U-shaped nanoparticle has its conversion peak at 0° , both the I- and T-shaped nanoparticles show maximum efficiency at oblique incidence. In particular, the T-shaped nanoparticle qualitatively behaves as a bare metal film, reaching a maximum second-harmonic enhancement at large angles ($\theta \simeq 70^\circ$), as shown in Fig. 7(b). The I-shaped nanoparticle shows a more interesting response. It reaches a conversion efficiency that overtakes the enhancement obtained with the U-shaped nanoparticle around $\theta \simeq 40^\circ$. An analysis of the linear transmission shows that the second resonance [see

Fig. 7(a)] redshifts as θ increases, attaining the wavelength $\lambda_{\text{FF}}/2$ for $\theta \simeq 40^\circ$, exactly where the maximum conversion occurs. The energy flowing from the pump to the second-harmonic field is then catalyzed, thanks to the presence of this double resonance, as shown in Fig. 7(a). The situation differs slightly for the T-shaped nanoparticle, where the resonances are matched only for wide angles, when the x component of the electric field, the one that drives the resonance, is sensibly reduced.

Another interesting structure to study is the nanocrescent. This structure has been shown to be able to efficiently harvest light over a broadband spectrum.⁸⁶ Moreover, its inherent asymmetry makes it a good candidate for second-harmonic generation enhancement. In Fig. 8(a) we show the fundamental and second-harmonic field distributions for 120-nm-wide periodically arranged nanocrescents. The nanocrescent was designed to reach a maximum sharpness defined by a minimum allowed size δ and to have a gap of size 2δ . The structure is excited by a fundamental wave polarized along the horizontal direction, as shown in Fig. 8(b). Similarly to the U-shaped nanoparticle, the symmetry breaking occurs along the y direction, the polarization state of the generated field results then rotated by 90° . The structure shows a maximum conversion efficiency at normal incidence that can enhance the second-harmonic generation process up to two orders of magnitude over that of the U-shaped nanoparticle efficiency. In particular, we obtained conversion efficiencies of $\eta \sim 6.0 \times 10^{-8}$, $\eta \sim 3.5 \times 10^{-8}$, and $\eta \sim 5.1 \times 10^{-9}$ for $\delta = 2, 3, 5$ nm, respectively, corresponding to a pumping peak intensity of ~ 55 MW/cm².

IV. CONCLUSION

We have studied the second-harmonic generation from metal-based nanostructures. The nonlinear optical response of metal was described using the hydrodynamic model, which introduced a source of nonlocality in the dispersion relation, due to electron gas pressure. We have discussed its influence on second-harmonic generation and numerically showed that, as the pressure term tends to zero, the amount of converted second-harmonic field tends to an asymptotic value, leading to the possibility of expressing the nonlinear surface contributions as a function of the values of the polarization vector in the bulk region. This development simplifies the investigation of second-harmonic generation process in full 3D metal structures.

Recent experimental work has shown significant enhancement of the electric field in plasmonic systems when metal nanoparticles are strongly coupled to a metal film.^{76,87} As the distances between the nanoparticles and the film approach the scale of fraction of a nanometer nonlocal effects are no longer negligible, and nonlinear effects become stronger. We believe that the ability to solve the full electromagnetic-hydrodynamic problem is crucial for this kind of system and will be the subject of our future investigations.

ACKNOWLEDGMENTS

The authors thank Yaroslav Urzhumov for valuable discussions. This work was supported by the Air Force Office of

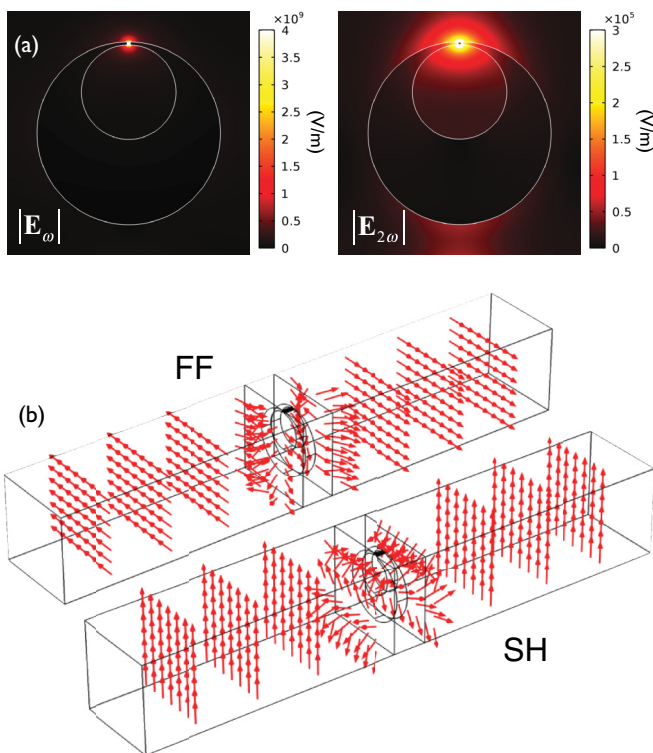


FIG. 8. (Color online) (a) Fundamental and second-harmonic field distributions for 150-nm-wide and 20-nm-thick gold nanocrescent arranged in a periodical array. (b) Electric field polarization state for the fundamental and second-harmonic fields, respectively. The polarization state of the generated field is flipped with respect to the pumping field.

Scientific Research (AFOSR, Grant No. FA9550-09-1-0562) and by the Army Research Office through a Multidisciplinary University Research Initiative (Grant No. W911NF-09-1-0539).

APPENDIX: NONLOCAL WEAK CONTRIBUTION

Consider a differential problem of the form $Lu = f$ with L a linear differential operator and f an arbitrary function. The associated weak form is then

$$\int_{\Omega} \varphi Lu \, dV = \int_{\Omega} \varphi f \, dV, \quad (\text{A1})$$

with $u|_{\partial\Omega} = u_0$, where φ is an element of a set of arbitrary functions called test functions. Generally, the form of the integrals of Eq. (A1) allows us to decrease the order of derivatives of the operator L . Here, we present a suitable weak form for the problem of Eqs. (6).

For the sake of simplicity, we rewrite here only differential higher-order terms, since lower ones remain unchanged. Consider, first, the term associated with the linear electron pressure $\nabla(\nabla \cdot \mathbf{P})$. Multiplying for the vectorial test function Φ and integrating over the volume as in Eq. (A1), we obtain

$$\int_{\Omega} \Phi \cdot [\nabla(\nabla \cdot \mathbf{P})] \, dV. \quad (\text{A2})$$

Integrating by parts and using the divergence theorem, we obtain

$$\begin{aligned} & \int_{\Omega} \Phi \cdot [\nabla(\nabla \cdot \mathbf{P})] \, dV \\ &= \int_{\partial\Omega} (\nabla \cdot \mathbf{P}) \mathbf{n} \cdot \Phi \, dA - \int_{\Omega} (\nabla \cdot \Phi)(\nabla \cdot \mathbf{P}) \, dV. \end{aligned} \quad (\text{A3})$$

Finally, considering that $\Phi \cdot \mathbf{n} = 0$ on the boundaries, we obtain

$$\int_{\Omega} \Phi \cdot [\nabla(\nabla \cdot \mathbf{P})] \, dV = - \int_{\Omega} (\nabla \cdot \Phi)(\nabla \cdot \mathbf{P}) \, dV. \quad (\text{A4})$$

Analogously, we obtain, for the nonlinear pressure term, $(\nabla \cdot \mathbf{P}) \nabla(\nabla \cdot \mathbf{P})$, of Eq. (6b) the following result:

$$\int_{\Omega} \Phi \cdot [(\nabla \cdot \mathbf{P}) \nabla(\nabla \cdot \mathbf{P})] \, dV = - \frac{1}{2} \int_{\Omega} (\nabla \cdot \Phi)(\nabla \cdot \mathbf{P})^2 \, dV, \quad (\text{A5})$$

where we used the identity

$$(\nabla \cdot \mathbf{P}) \nabla(\nabla \cdot \mathbf{P}) = \frac{1}{2} \nabla(\nabla \cdot \mathbf{P})^2. \quad (\text{A6})$$

The surface currents given by Eq. (9) have been implemented by using surface contributions.

*cristian.ciraci@duke.edu

¹D. Schurig, J. J. Mock, B. J. Justice, S. A. Cummer, J. B. Pendry, A. F. Starr, and D. R. Smith, *Science* **314**, 977 (2005).

²D. R. Smith and N. Kroll, *Phys. Rev. Lett.* **85**, 2933 (2000).

³I. V. Shadrivov, A. B. Kozyrev, D. van der Weide, and Y. S. Kivshar, *Opt. Express* **16**, 20266 (2008).

⁴A. A. Zharov, I. V. Shadrivov, and Y. S. Kivshar, *Phys. Rev. Lett.* **91**, 037401 (2003).

⁵S. O'Brien, D. McPeake, S. A. Ramakrishna, and J. B. Pendry, *Phys. Rev. B* **69**, 241101 (2004).

⁶E. Poutrina, D. Huang, and D. R. Smith, *New J. Phys.* **12**, 093010 (2010).

⁷S. Larouche and D. R. Smith, *Opt. Commun.* **283**, 1621 (2010).

⁸A. Rose, S. Larouche, D. Huang, E. Poutrina, and D. R. Smith, *Phys. Rev. E* **82**, 036608 (2010).

⁹J. Zhou, T. Koschny, M. Kafesaki, E. N. Economou, J. B. Pendry, and C. M. Soukoulis, *Phys. Rev. Lett.* **95**, 223902 (2005).

¹⁰R. W. Boyd and G. L. Fischer, in *Encyclopedia of Materials: Science and Technology* (Elsevier Science Ltd., Amsterdam, 2001), pp. 6237–6244.

¹¹P. A. Franken, G. Weinreich, C. W. Peters, and A. E. Hill, *Phys. Rev. Lett.* **7**, 118 (1960).

¹²N. Bloembergen and P. S. Pershan, *Phys. Rev.* **128**, 606 (1961).

¹³P. S. Pershan, *Phys. Rev.* **130**, 919 (1963).

¹⁴P. A. Franken and J. Ward, *Rev. Mod. Phys.* **35**, 23 (1962).

¹⁵N. Bloembergen, *Proc. IEEE* **51**, 124 (1963).

¹⁶E. Adler, *Phys. Rev.* **134**, A728 (1964).

¹⁷N. Bloembergen, R. Chang, S. Jha, and C. Lee, *Phys. Rev.* **174**, 813 (1968).

¹⁸F. Brown, R. Parks, and A. Sleeper, *Phys. Rev. Lett.* **14**, 1029 (1965).

¹⁹S. Jha, *Phys. Rev. Lett.* **15**, 412 (1965).

²⁰H. Sonnenberg and H. Heffner, *J. Opt. Soc. Am. A* **58**, 209 (1968).

²¹J. C. Quail and H. J. Simon, *Phys. Rev. B* **31**, 4900 (1985).

²²J. Coutaz, D. Maystre, M. Neviere, and R. Reinisch, *J. Appl. Phys.* **62**, 1529 (1987).

²³H. J. Simon, C. Huang, J. C. Quail, and Z. Chen, *Phys. Rev. B* **38**, 7408 (1988).

²⁴D. Krause, C. W. Teplin, and C. T. Rogers, *J. Appl. Phys.* **96**, 3626 (2004).

²⁵S. Jha, *Phys. Rev.* **140**, A2020 (1965).

²⁶N. Bloembergen and Y. Shen, *Phys. Rev.* **141**, 298 (1966).

²⁷P. Guyot-Sionnest, W. Chen, and Y. R. Shen, *Phys. Rev. B* **33**, 8254 (1986).

²⁸F. Brown and R. Parks, *Phys. Rev. Lett.* **16**, 507 (1966).

²⁹A. Liebsch, *Phys. Rev. Lett.* **61**, 1233 (1988).

³⁰J. I. Dadap, J. Shan, K. B. Eisenthal, and T. F. Heinz, *Phys. Rev. Lett.* **83**, 4045 (1999).

³¹M. I. Stockman, D. J. Bergman, C. Anceau, S. Brasselet, and J. Zyss, *Phys. Rev. Lett.* **92**, 057402 (2004).

³²K. Li, M. I. Stockman, and D. J. Bergman, *Phys. Rev. B* **72**, 153401 (2005).

³³G. Bachelier, I. Russier-Antoine, E. Benichou, C. Jonin, and P.-F. Brevet, *J. Opt. Soc. Am. B* **25**, 955 (2008).

³⁴J. Rudnick and E. Stern, *Phys. Rev. B* **4**, 4274 (1971).

³⁵J. E. Sipe, V. C. Y. So, M. Fukui, and G. I. Stegeman, *Phys. Rev. B* **21**, 4389 (1980).

³⁶M. Corvi and W. L. Schaich, *Phys. Rev. B* **33**, 3688 (1986).

³⁷C. D. Hu, *Phys. Rev. B* **40**, 7520 (1989).

³⁸M. Airola, Y. Liu, and S. Blair, *J. Opt. A* **7**, S118 (2005).

- ³⁹A. Lesuffleur, L. K. S. Kumar, and R. Gordon, *Appl. Phys. Lett.* **88**, 261104 (2005).
- ⁴⁰J. A. H. van Nieuwstadt, M. Sandtke, R. H. Harmsen, F. B. Segerink, J. C. Prangma, S. Enoch, and L. Kuipers, *Phys. Rev. Lett.* **97**, 146102 (2006).
- ⁴¹M. A. Vincenti, V. Petruzzelli, A. D’Orazio, F. Prudenzeno, M. J. Bloemer, N. Akozbek, and M. Scalora, *J. Nanophotonics* **2**, 021851 (2008).
- ⁴²T. Xu, X. Jiao, and S. Blair, *Opt. Express* **17**, 23582 (2009).
- ⁴³M. A. Vincenti, D. de Ceglia, V. Roppo, and M. Scalora, *Opt. Express* **19**, 2067 (2011).
- ⁴⁴M. C. Larciprete, A. Belardini, M. G. Cappeddu, D. de Ceglia, M. Centini, E. Fazio, C. Sibilia, M. J. Bloemer, and M. Scalora, *Phys. Rev. A* **77**, 013809 (2008).
- ⁴⁵G. D’Aguanno, M. C. Larciprete, N. Mattiucci, A. Belardini, M. J. Bloemer, E. Fazio, O. Buganov, M. Centini, and C. Sibilia, *Phys. Rev. A* **81**, 013834 (2010).
- ⁴⁶K. D. Ko, A. Kumar, K. H. Fung, R. Ambekar, G. L. Liu, N. Fang, and K. C. Toussaint, *Nano Lett.* **11**, 61 (2011).
- ⁴⁷A. Benedetti, M. Centini, C. Sibilia, and M. Bertolotti, *J. Opt. Soc. Am. B* **27**, 408 (2010).
- ⁴⁸A. Belardini, M. C. Larciprete, M. Centini, E. Fazio, C. Sibilia, M. Bertolotti, A. Toma, D. Chiappe, and F. B. de Mongeot, *Opt. Express* **17**, 3603 (2009).
- ⁴⁹J. Renger, R. Quidant, N. van Hulst, and L. Novotny, *Phys. Rev. Lett.* **104**, 046803 (2010).
- ⁵⁰M. W. Klein, C. Enkrich, M. Wegener, and S. Linden, *Science* **313**, 502 (2006).
- ⁵¹F. B. P. Niesler, N. Feth, S. Linden, J. Niegemann, J. Gieseler, K. Busch, and M. Wegener, *Opt. Lett.* **34**, 1997 (2009).
- ⁵²C. C. Neacsu, G. A. Reider, and M. B. Raschke, *Phys. Rev. B* **71**, 201402(R) (2005).
- ⁵³J. Nappa, G. Revillod, I. Russier-Antoine, E. Benichou, C. Jonin, and P. F. Brevet, *Phys. Rev. B* **71**, 165407 (2005).
- ⁵⁴J. Shan, J. I. Dadap, I. Stiopkin, G. A. Reider, and T. F. Heinz, *Phys. Rev. A* **73**, 023819 (2006).
- ⁵⁵M. Zavelani-Rossi, M. Celebrano, P. Biagioni, D. Polli, M. Finazzi, L. Duò, G. Cerullo, M. Labardi, M. Allegrini, J. Grand, and P. Adam, *Appl. Phys. Lett.* **92**, 093119 (2008).
- ⁵⁶J. Butet, J. Duboisset, G. Bachelier, I. Russier-Antoine, E. Benichou, C. Jonin, and P.-F. Brevet, *Nano Lett.* **10**, 1717 (2010).
- ⁵⁷B. K. Canfield, S. Kujala, K. Jefimovs, J. Turunen, and M. Kauranen, *Opt. Express* **12**, 5418 (2004).
- ⁵⁸M. W. Klein, M. Wegener, N. Feth, and S. Linden, *Opt. Express* **15**, 5238 (2006).
- ⁵⁹M. D. McMahon, R. Lopez, R. F. Haglund, E. A. Ray, and P. H. Bunton, *Phys. Rev. B* **73**, 041401(R) (2006).
- ⁶⁰B. K. Canfield, H. Husu, J. Laukkanen, B. Bai, M. Kuittinen, J. Turunen, and M. Kauranen, *Nano Lett.* **7**, 1251 (2007).
- ⁶¹C. Hubert, L. Billot, P. Adam, R. Bachelot, P. Royer, J. Grand, D. Gindre, K. D. Dorkenoo, and A. Fort, *Appl. Phys. Lett.* **90**, 181105 (2007).
- ⁶²N. Feth, S. Linden, M. W. Klein, M. Decker, F. B. P. Niesler, Y. Zeng, W. Hoyer, J. Liu, S. W. Koch, J. V. Moloney, and M. Wegener, *Opt. Lett.* **33**, 1975 (2008).
- ⁶³H. Husu, B. K. Canfield, J. Laukkanen, B. Bai, M. Kuittinen, J. Turunen, and M. Kauranen, *Appl. Phys. Lett.* **93**, 183115 (2008).
- ⁶⁴E. Kim, F. Wang, W. Wu, Z. Yu, and Y. R. Shen, *Phys. Rev. B* **78**, 113102 (2008).
- ⁶⁵S. Kujala, B. K. Canfield, M. Kauranen, Y. Svirko, and J. Turunen, *Opt. Express* **16**, 17196 (2008).
- ⁶⁶V. K. Valev, N. Smisdom, A. V. Silhanek, B. de Clercq, W. Gillijns, M. Ameloot, V. V. Moshchalkov, and T. Verbiest, *Nano Lett.* **9**, 3945 (2009).
- ⁶⁷V. K. Valev, A. V. Silhanek, N. Smisdom, B. de Clercq, W. Gillijns, O. Aktsipetrov, M. Ameloot, V. V. Moshchalkov, and T. Verbiest, *Opt. Express* **18**, 8286 (2010).
- ⁶⁸V. K. Valev, A. V. Silhanek, N. Verellen, W. Gillijns, P. van Dorpe, O. A. Aktsipetrov, G. A. E. Vandenbosch, V. V. Moshchalkov, and T. Verbiest, *Phys. Rev. Lett.* **104**, 127401 (2010).
- ⁶⁹T. Utikal, T. Zentgraf, T. Paul, C. Rockstuhl, F. Lederer, M. Lippitz, and H. Giessen, *Phys. Rev. Lett.* **106**, 133901 (2011).
- ⁷⁰Y. Zeng, W. Hoyer, J. Liu, S. W. Koch, and J. V. Moloney, *Phys. Rev. B* **79**, 235109 (2009).
- ⁷¹M. Scalora, M. A. Vincenti, D. de Ceglia, V. Roppo, M. Centini, N. Akozbek, and M. J. Bloemer, *Phys. Rev. A* **82**, 043828 (2010).
- ⁷²C. Ciraci, E. Poutrina, M. Scalora, and D. R. Smith, *Phys. Rev. B* **85**, 201403(R) (2012).
- ⁷³A. Eguiluz and J. Quinn, *Phys. Rev. B* **14**, 1347 (1976).
- ⁷⁴N. Crouseilles, P.-A. Hervieux, and G. Manfredi, *Phys. Rev. B* **78**, 155412 (2008).
- ⁷⁵R. W. Boyd, *Nonlinear Optics* (Academic Press, San Diego, CA, 2006).
- ⁷⁶C. Ciraci, R. T. Hill, J. J. Mock, Y. A. Urzhumov, A. I. Fernández-Domínguez, S. A. Maier, J. B. Pendry, A. Chilkoti, and D. R. Smith, *Science* **337**, 1072 (2012).
- ⁷⁷R. Ruppín, *Opt. Commun.* **190**, 205 (2001).
- ⁷⁸S. Raza, G. Toscano, A.-P. Jauho, M. Wubs, and N. A. Mortensen, *Phys. Rev. B* **84**, 121412 (2011).
- ⁷⁹J. M. McMahon, S. K. Gray, and G. C. Schatz, *Phys. Rev. Lett.* **103**, 097403 (2009).
- ⁸⁰P. Halevi and R. Fuchs, *J. Phys. C* **17**, 3889 (1984).
- ⁸¹D. Maystre, M. Neviere, and R. Reinisch, *Appl. Phys. A* **39**, 115 (1986).
- ⁸²P. Jewsbury, *J. Phys. F* **11**, 195 (1981).
- ⁸³COMSOL Multiphysics, <http://www.comsol.com/>.
- ⁸⁴K. O’Donnell and R. Torre, *New J. Phys.* **7**, 154 (2005).
- ⁸⁵M. W. Klein, M. Wegener, N. Feth, and S. Linden, *Opt. Express* **16**, 8055 (2008).
- ⁸⁶A. Aubry, D. Y. Lei, A. I. Fernández-Domínguez, Y. Sonnefraud, S. A. Maier, and J. B. Pendry, *Nano Lett.* **10**, 2574 (2010).
- ⁸⁷R. T. Hill, J. J. Mock, Y. A. Urzhumov, D. S. Sebban, S. J. Oldenburg, S.-Y. Chen, A. A. Lazarides, A. Chilkoti, and D. R. Smith, *Nano Lett.* **10**, 4150 (2010).